Sulfur-doped carbon/TiO_2 composites for ethylene photo-oxidation. Enhanced performance by doping TiO_2 phases with sulfur by mobile species inserted on the carbon support

Lorena T. Pérez-Poyatos, Sergio Morales-Torres, Luisa M. Pastrana-Martínez*, Francisco J. Maldonado-Hódar

NanoTech – Nanomaterials and Sustainable Chemical Technologies, Department of Inorganic Chemistry, Faculty of Sciences, University of Granada, Avda. Fuente Nueva s/n, ES18071 Granada, Spain.

**Corresponding author: lpastrana@ugr.es (Luisa M Pastrana-Martínez), Tlf. +34 958248489.*

Abstract

The performance of carbon xerogel/TiO_2 composites in ethylene photo-oxidation was analyzed under dynamic conditions considering various parameters, namely sulfur doping, dry *vs.* humid conditions and type of radiation (ultraviolet, UV, *vs.* visible light, Vis). The catalysts were synthesized using an acid-catalyzed sol-gel process and characterized with complementary techniques, including SEM/EDX, XRD, XPS and physical adsorption of N_2 and CO_2, among others. The performance of samples in ethylene removal by adsorption and photo-oxidation under dynamic flow was discussed and related with their physicochemical properties and the experimental conditions. Although ethylene adsorption was hindered by doping and humidity, both factors were found to enhance photoactivity by promoting the formation of highly oxidant hydroxyl radicals ($HO^•$). The composites showed an improved catalytic performance compared to bare TiO_2, with sulfur improving the activity by approximately 8%. The presence of the carbon material also enhanced the performance under Vis radiation by nearly 25%. It was suggested that sulfur species could migrate from the carbon support to the TiO_2 nanoparticles during carbonization, forming Ti-O-S bonds. This finding constitutes a novel, cost-effective, sustainable and scalable method for the preparation of supported and doped TiO_2 nanocomposites.

***Keywords**: Carbon xerogel; sulfur doping; TiO_2; ethylene; adsorption; heterogeneous photocatalysis.*

1. Introduction

TiO_2 remains one of the most widely used photoactive materials, although its high band gap (BG) value limits its efficiency under solar radiation. To overcome this limitation, BG values can be reduced by introducing defects into the crystal structure, either through the creation of vacancies (e.g. black titania) [1-3] or by doping with metallic (Ag, Au) [4, 5] and non-metallic (N, P, C, S) elements [6-9].

Doping carbon or TiO_2 phases with sulfur species is a well-established approach that remains of great interest due to its applications in electro-photochemistry. Different methods have been used to prepare S-TiO_2 materials, including the oxidation annealing of TiS_2 [10], flame spray pyrolysis [11] or hydrothermal treatments [12]. Metalorganic chemical vapor deposition (MOCVD) is also effective to prepare TiO_2 films. The adsorption of H_2S onto the TiO_2 surface can be conducted under atmospheric pressure at low temperatures [13]. Hydroxyl radicals ($HO^{\bullet}$) on the surface of TiO_2 films can oxidize adsorbed H_2S to form SO_4^{2-} groups. The sulfur atomic concentration in the films decreases from 8.0% to 0.2% as the doping temperature increases up to 150 ºC. The TiO_2 structure remains as anatase after sulfur doping but the formation of Ti–O–S bonds indicate the substitution of Ti^{4+} ions by S^{6+} in the lattice, while SO_4^{2-} groups are formed on the surface. Bayati and co-workers [6] reported a micro-arc oxidation process with sodium thiosulfate ($Na_2S_2O_3{\cdot}5H_2O$) solution with different concentrations as electrolyte to achieve a sulfur doping range of 0.14% to 1.23% wt. by adjusting the voltage between 300 and 550 V. XPS analysis detected only Ti^{4+} but the binding energy (BE) in the Ti(2p) spectral region showed a slight shift toward lower binding energies after doping. X-ray diffraction (XRD) peaks of anatase and rutile shifted to higher diffraction angles, indicating that sulfur doping occurred through the substitution of Ti^{4+} with cationic S^{4+} or S^{6+}, since the substitution of O^{2-} by larger anion S^{2-} would, conversely, increase interlayer spaces and decrease diffraction angles. The BG of TiO_2 decreased progressively with the S-content up to a value of 2.29 eV, although the best catalytic performance was found for intermediate values. This outcome is influenced by additional factors, such as porosity, and as sulfur content increases, new energetic states appear on the valence band (VB) that are progressively closer to the conduction band (CB).

In this manuscript, two strategies to enhance the TiO_2 performance under solar radiation were combined: (i) reducing the TiO_2 particle size by forming nanocrystals on a suitable porous support; and (ii) doping with non-metallic sulfur (S) heteroatoms. The synergistic effect between TiO_2 and carbon phase in developing photocatalysts has been previously demonstrated using various carbon materials, including graphene [14, 15], carbon nanotubes and carbon nanofullerenes (CNTs-CNF) [16] and classical activated carbon [17]. In this case, carbon xerogel/TiO_2 nanocomposites were prepared by carbonization of the polymers obtained by a sol-gel method. Carbon gels and their composites are typically prepared through the condensation of resorcinol – formaldehyde [18, 19]. This mixture of reactants was used as reference materials for the carbon phase. However, using thiophene-2-carboxaldehyde as a polymerizing agent with resorcinol molecules results in the formation of sulfur-doped polymers. Both doped and undoped polymers were impregnated with Ti-alkoxide as precursor of TiO_2 phase, forming the corresponding composites after carbonization. The influence of sulfur in the organic polymer on both the physicochemical characteristics and the adsorptive/photocatalytic performance of the composites (with or without humidity) was analyzed.

Ethylene was selected as the target volatile organic compound (VOC) due to its significance in devices storing climacteric fruits. The removal of ethylene is currently of great technological importance for optimizing the ripening degree and preserving the organoleptic properties of the fruit. Photocatalysis is a promising technology for this purpose in the agrifood industry [17, 20].

2. Methodology

2.1 Carbon xerogels/TiO_2 composites synthesis

The bare and composite xerogels were synthesized by a sol-gel method, using HCl as polymerization catalyst. The organic polymer was formed at 75 ºC in acidic medium and with a resorcinol (R)/thiophene-2-carboxaldehyde/water molar ratio of 1/2/8 (i.e., CXS sample). For the synthesis of the reference xerogel, thiophene-2-carboxaldehyde was substituted by formaldehyde (F) (i.e., CX sample). The TiO_2 phase was synthesized using Ti(IV) isopropoxide to provide a carbon/TiO_2 proportion of 50% in the final composite. Samples were carbonized at 800 ºC under N_2 atmosphere. The composites were labelled as CX-TiO_2 and CXS-TiO_2 when using CX or CXS xerogels, respectively. Additional details are summarized in the supplementary material (SM) section.

2.2 Materials characterization

Catalysts were extensively characterized with different complementary techniques, such as thermogravimetric analysis (TGA), physical adsorption of N_2 and CO_2, pH at point of zerocharge (pH_{PZC}), scanning electron microscopy (SEM) and energy dispersive X-ray spectroscopy (EDX), X-ray diffraction (XRD), X-ray photoelectron spectroscopy (XPS) and UV-Vis diffuse reflectance (DRUV), as described in the SM section.

2.3 Adsorption and photocatalytic experiments

The adsorption experiments were conducted under dynamic conditions at previously reported experimental set-up [17]. A total flow of 25 mL/s of air containing 100 ppm of ethylene passes throughout the column and is analyzed at the outlet by gas chromatography (GC) using a Shimadzu GC 2010 Plus to obtain the breakthrough curves [17, 21]. Experiments were also carried out with a relative humidity (RH) of 50% to determine the influence of the humidity. For the photocatalytic experiments, once the samples were saturated, the column was irradiated using a medium-pressure mercury lamp (125 W, model 3010/PX0686, Photochemical Reactors LTD). The experiments were carried out under UV and visible irradiation and in the presence and absence of humidity. Further details can be found in the SM section.

3. Results and discussion

3.1 Characterization of the carbon xerogels/TiO_2 composites

The TiO_2 content on CX-TiO_2 and CXS-TiO_2 was determined by TGA (Figure S1, SM). The recipes were fitted to provide around 50% wt. of each carbon and TiO_2 phase, assuming a mean weight loss (WL) of around 55% during carbonization of the organic fraction. Anyway, the TiO_2 loading slightly exceeded the 50% in CX-TiO_2 (54% wt.) and is smaller on CXS-TiO_2 (46% wt.), thus the TiO_2 content between samples differs in around 10% wt. TGA profiles in air (Figure S1) show a great thermal stability of both composites, which even improves after S-doping. The combustion of the carbon phase is negligible below 400 ºC, suggesting that these materials could be also used as catalysts or catalyst support in thermal combustion processes of VOCs.

The morphology and chemical characteristics of the carbon xerogel-TiO_2 composites (CX-TiO_2 and CXS-TiO_2) were analyzed by SEM/EDX (Figure 1). The presence of surfactant in the starting solution induces the formation of spherical particles with a mean diameter of around 20 μm of organic RF polymers. These structures are formed by overlapped and spherical particles with a cross-linked-like structure, known as primary particles. These microspheres are then coated with TiO_2 by hydrolysis of the added alkoxide during the synthesis process, as described in the experimental section. After carbonization, this results in a well-dispersed distribution of small TiO_2 particles on the structured carbon supports for the CX-TiO_2 composite (Figure 1a).

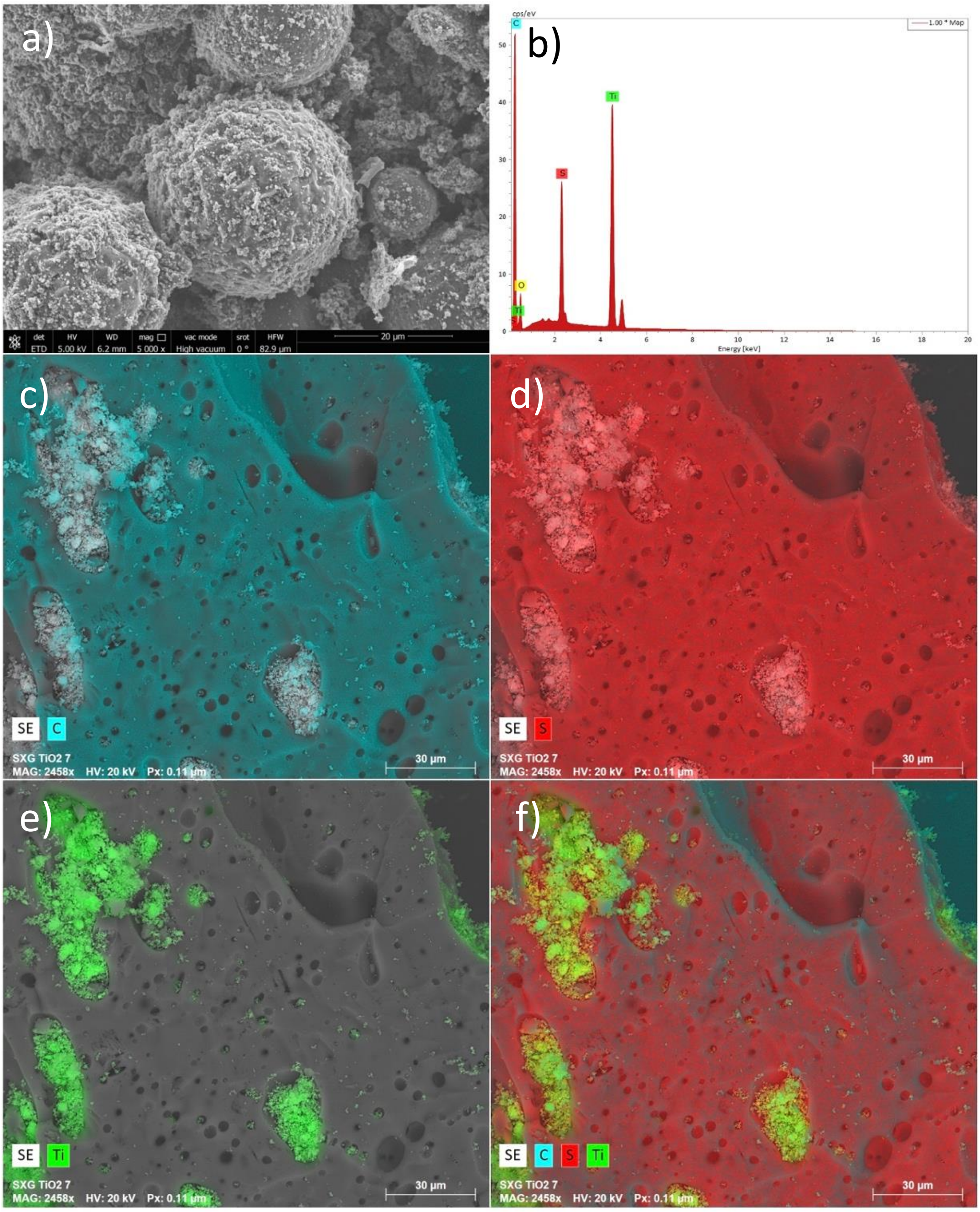

Figure 1. a) Morphology of CX-TiO_2 sample; b) EDX analysis and c), d), e) and f) mapping of the chemical composition of CXS-TiO_2 composite.

In the case of the S-doped composite (CXS-TiO_2), EDX analysis confirms the presence of S-species after carbonization at 800 ºC (Figure 1b). Figures 1c-f show the mapping for the elemental analysis (C, Ti, S) for a selected area around an agglomeration of supported TiO_2 particles in the CXS-TiO_2 composite. Because the S-functionalities were introduced in the organic xerogel, it was expected that they remained in the derivative carbon xerogel phase. However, when analyzing the obtained results, a preferential localization of S-species is observed on the TiO_2 particles, rather than on the carbon support (Figure 1f). The simultaneous carbonization of the organic polymers and TiO_2 phases in the raw composite may have allowed sulfur species to migrate from the organic phase to the oxide phase during the process. During carbonization, gaseous SH_x- or SO_x- species are likely formed along with other pyrolysis gases (CO_x, CH_x). This contributes to a higher weight loss in CXS-TiO_2 compared to CX-TiO_2 (see TGA results, Figure S1), allowing gaseous S-species to be re-adsorbed on the TiO_2 particles [22, 23]. Nevertheless, the possibility of solid-state reactions cannot be ruled out. The high dispersion of TiO_2 on the organic polymer ensures a good contact between both phases and the elevated carbonization temperature can promote atomic diffusion of sulfur between adjacent particles. This mechanism is also supported by the very small size of TiO_2 crystallites, which likely have a high degree of imperfections and highly reactive boundaries within the polycrystalline TiO_2 phase. In fact, the XRD of un-carbonized composites (results not shown) are characterized by the absence of peaks, denoting a clear lack of crystallinity. Developing new strategies for doping carbon and TiO_2 with sulfur functionalities is currently a trending topic in the field of materials for electrochemical applications, among others [24-26].

The textural characteristics of samples were analyzed by combining the information from N_2 and CO_2 adsorption. In absence of diffusional restriction, the amount of N_2 adsorbed at $P/P_0 = 0.95$ is considered as the total pore volume (V_T) [27]. However, the N_2 diffusion at -196 ºC is too slow and when narrow micropores are present the porosity and surface area determined by this technique can be underestimated. However, this porosity is accessible to the CO_2 at 0 ºC, thus providing complementary information of the whole porosity range.

The corresponding N_2 and CO_2 adsorption isotherms are showed in Figures S2a and b, respectively, and the determined Brunauer, Emmet and Teller (BET) surface area (S_{BET}), total pore volume (V_T), mesoporous and micropore volume (V_{meso} and W_0, respectively), among others are listed in Table S1 (SM). The characteristics of bare TiO_2 and carbon phases were also included for comparison. The N_2-adsorption isotherm of TiO_2 denotes the absence of adsorption at low

P/P_0 values, only increasing slowly at P/P_0 >0.4, indicating the absence of microporosity and only the formation of a certain volume between particles. On the contrary, the carbon xerogel from R-F (CX sample) is the most porous sample in the series, showing a type II - IV N_2-adsorption isotherm, which indicates a well-developed micro- and mesoporosity. The different aldehyde used in the polymerization for the CXS sample, influences not only the surface chemistry, as previously discussed, but also the pore size distribution (PSD) as denoted by the changes in the isotherm profiles, also in agreement with previous studies [22]. The CX sample exhibits a high micro- and mesoporous volume but has a small mean micropore width (L_0), Table S1. On the other hand, CXS sample displays more heterogeneous microporosity, characterized by large micropores, and, as a result, a lower microporous surface (S_{mic}). In both cases, the porosity of both composites (i.e., CX-TiO_2 and CXS-TiO_2) decreases regarding the corresponding carbon gel due to the very low porosity of the oxide phase.

After doping with the TiO_2 phase, the W_0 values determined by CO_2 adsorption significantly decreased, while L_0 only slightly increased (Figure S2b and Table S1). However, L_0 determined from N_2 adsorption, increased for CX samples (from 0.81 nm to 1.48 nm for CX and CX-TiO_2, respectively) and slightly decreased for CXS (from 1.70 nm to 1.58 nm for CXS and CXS-TiO_2, respectively). This suggests that TiO_2 nanoparticles are located inside the pores with diameter higher than 1.7 nm, thus reducing L_0, and also in pores with diameters smaller than 0.8 nm. Consequently, TiO_2 mainly blocks the microporosity on CX, leading to a significant reduction of S_{mic}, and affecting the narrow microporosity as determined by CO_2 adsorption. Since TiO_2 particles are formed only on the external surface of the organic polymers working as support, they will be accessible during the photocatalytic processes. Furthermore, both composites maintain significantly high S_{BET} areas and well-developed meso/microporous character compared to bare TiO_2, which also favors the ethylene adsorption.

The crystallographic characteristics of TiO_2 and both CX-TiO_2 and CXS-TiO_2 composites were analyzed by XRD (Table 1 and Figure S3, SM). Due to the high treatment temperature of 800 ºC used in all samples, TiO_2 exhibited a highly crystalline rutile phase (Figure S3). The lower intensity of the XRD peaks in the composites is related to the dilution effect. Nevertheless, the significant widening of the XRD peaks confirms the smaller crystallinity of TiO_2 in the composites, as denoted also by the variations of the mean crystallite size calculated by applying the Scherrer equation (Table 1). Additionally, in the composites, TiO_2 is forming a mixture of crystalline anatase/rutile phases. Thus, the support partially preserves the TiO_2 dispersion at elevated temperature, avoiding sintering and the transformation of the crystallographic phase from anatase to rutile. This behavior was observed in different series of samples [28, 29]. During thermal treatment, small anatase particles aggregate and transform into rutile, with the rutile crystal size progressively increasing as the anatase fraction decreased. In this case, the presence of sulfur in the support clearly enhances these effects, since CXS-TiO_2 predominantly consists of anatase phase, while CX-TiO_2 is mainly composed of rutile, with a crystallite size of 9.3 nm and 17.0 nm, respectively (Table 1). The anatase/rutile ratio in CXS-TiO_2 is ten times greater than in CX-TiO_2 (1.35 and 0.17, respectively, Table 1) and it presents a smaller mean crystallite size of both rutile and anatase, Table 1. The smaller degree of transformation in CXS compared to CX also denotes a stronger interaction with the support when deposited on sulfur-doped carbon xerogels.

The surface composition of composites given by XPS is listed in Table 1. Doping with thiophene-2-carboxaldehyde not only introduces a certain amount of sulfur species (1.33%) but also significantly increases the oxygen content (10.35% and 16.96% for CX-TiO_2 and CXS-TiO_2, respectively). The higher oxygen content (%O) observed in CXS-TiO_2 compared to CX-TiO_2 can be attributed to the higher surface TiO_2 content (Table 1) as well as the smaller TiO_2 sintering as previously observed by XRD for this sample (Figure S3).

Table 1. Crystallite mean size (d_{rutile} and $d_{anatase}$), anatase/rutile (A/R) ratio and surface composition of the composites (obtained by XPS).

Sample	d_{rutile} (nm)	$d_{anatase}$ (nm)	A/R ratio	C (%)	O (%)	S (%)	Ti (%)
TiO_2	28.1	-	-	-	-	-	-
CX-TiO_2	17.0	9.5	0.17	87.18	10.35	-	2.47
CXS-TiO_2	13.7	9.3	1.35	77.03	16.96	1.33	4.68

The pH_{PZC} of bare TiO_2 is 4.6, which is mainly associated to its Lewis acidity [17] and was found in agreement with other works for rutile TiO_2 [30, 31]. CX-TiO_2 has a neutral character, with a pH_{PZC} of 7.0, while CXS-TiO_2, which also has a higher surface oxygen and titania content (Table 1), shows a slightly acidic pH_{PZC} of 6.8. This variation is consistent with the formation of acidic sulfur species (-SH or –SO_x).

High resolution XPS spectra of C1s, O1s, S2p and Ti2p regions of the composites were analyzed to study the nature of the surface chemical groups. The deconvolution of the different spectral regions allows a more specific comparison of the different types of surface groups present in each sample and their concentration. The results of the C1s region of the composites are summarized in Figure 2. The C1s spectra (Figure 2a and 2c) were deconvoluted into four components corresponding to the following bonds: C-C, C=C (284.6 eV); C-O (ca. 285 eV); C=O (ca. 286 eV) and O-C=O (ca. 289 eV). The component associated with the C-O bond overlaps with weaker signals of C-S bonds in the heteroatom-doped composite, which have a BE around 285 eV [22].

Regarding the deconvolution of the high-resolution O1s spectra (Figures 2b and 2d), three components were used to fit the CX-TiO_2 profile. The main component corresponds to Ti-O bonds, at binding energy of 530.5 eV [32], followed by two smaller components associated with the oxygen surface groups present on the carbon phase. These components at 531 eV and 533 eV are typically assigned to C=O and C-O bonds, respectively [22, 33]. In the case of CXS-TiO_2, an additional component at 532 eV was attributed to O-S species in a proportion of 15% (Figure 2d) [34].

The S2p region of the doped composite (CXS-TiO_2) exhibits a typical peak splitting between $S2p_{3/2}$ and $S2p_{1/2}$, with a BE difference of 1.2 eV (Figure 2e). The main component, observed at around 163.7 eV and accounting for 57%, is attributed to C-S-C bonds. This peak also overlaps with the signal corresponding to Ti-O-S bonds, due to the presence of metal sulfides [34]. Additional smaller components are observed at 164.3 eV and 167.5 eV, which are associated with H-S-C and oxidized sulfur moieties (such as sulfonates or sulfates), respectively [22, 35].

High-resolution XPS spectra of the Ti2p region were also analysed for both composites (Figure 2f and g). These spectra show the characteristic peak splitting between $Ti2p_{3/2}$ and $Ti2p_{1/2}$, with a binding energy difference of 5.7 eV. In both cases, only the Ti(IV) oxidation state is observed, indicating that no reduction of Ti occurs due to interaction with the organic fraction during pyrolysis. However, the BE in both cases differs, for CX-TiO_2, it appears at 458.5 eV, while for CXS-TiO_2 it is observed at 458.6 eV. This slight shift could be attributed to the different predominant crystalline phase in each sample, as discussed during XRD results [36]. The undoped sample consisted primary of rutile phase, whereas the S-doped sample exhibited a higher proportion of anatase, as shown in their anatase/rutile ratio (0.17 vs 1.35, respectively, Table 1).

The optical properties of the composites were analyzed by DRUV spectroscopy (Figure S4). The absorption spectra of the samples, transformed using the Kubelka–Munk equation, $F(R)= (1-R)^2/2R$, are shown in Figure S4a. TiO_2 presents the typical broad band of absorption below 400 nm and the shape and intensity of this band can be significantly influenced by the nature of supports used. The introduction of the carbon support increases the absorption threshold of the materials in both UV range and visible range (wavelengths above 380 nm), resulting in catalysts that can be active under visible light due to the synergistic effect between both phases [17, 37].

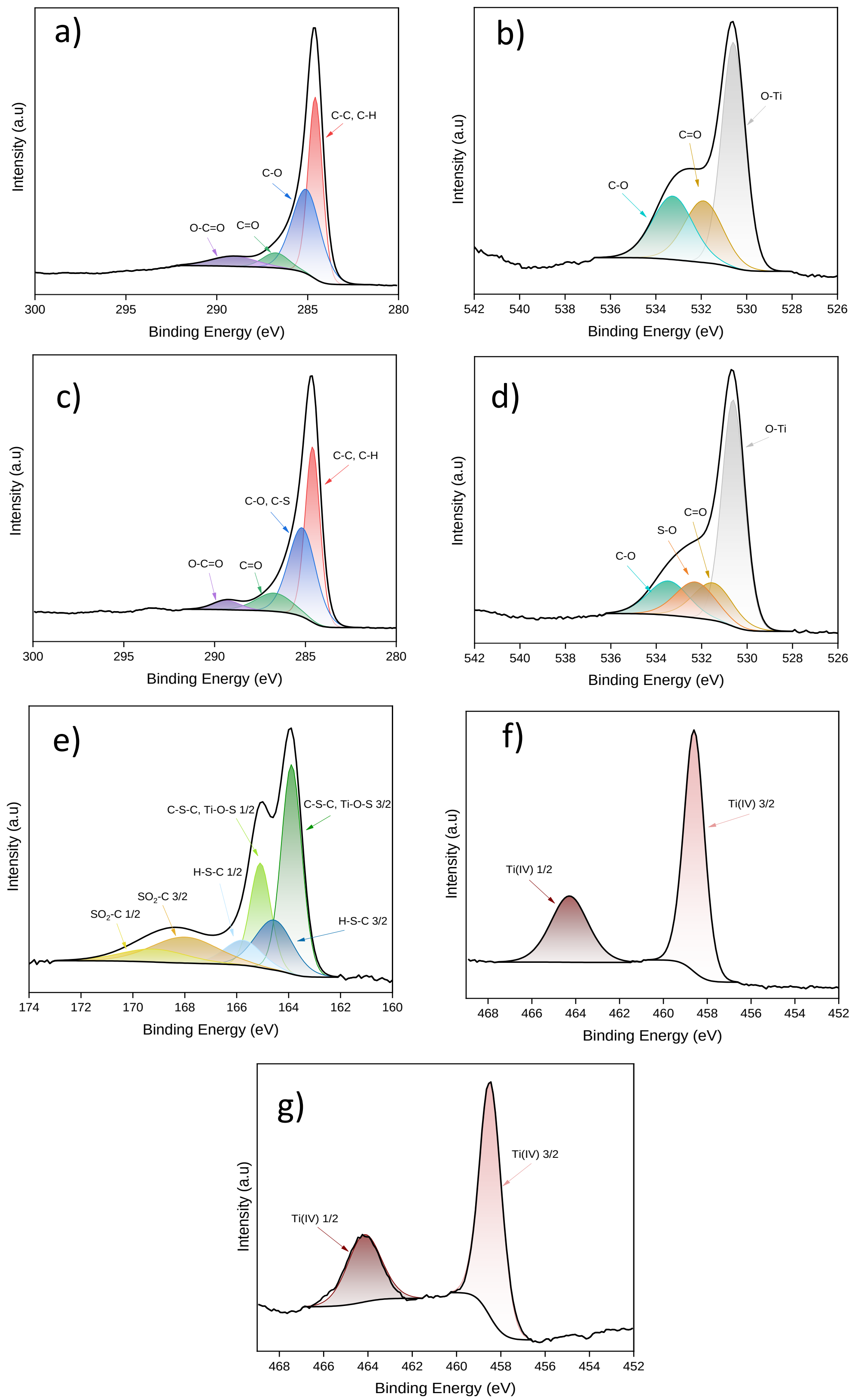

Figure 2. Deconvolution of a) C1s, b) O1s and g) Ti2p spectral regions of CX-TiO_2. Deconvolution of c) C1s, d) O1s, e) S2p and f) Ti2p spectral regions of CXS-TiO_2 composite.

Figure S4b displays the Tauc´s plots versus the energy (eV) and the calculated band gap energy (E_g). The TiO_2 phase presents different BG values depending on its phase; typical values around 3.2 eV are described for anatase and 3.0 eV for rutile [28, 38]. These values can also be influenced by other factors such as the presence of oxygen vacancies [3], nanostructures [17] and so on.

The BG value for bare TiO_2 was 3.0 eV, in good agreement with the well crystalized rutile phase, identified by XRD (Figure S3). Regarding the composites, a general reduction of this parameter is observed for the CXS-TiO_2 sample, exhibiting a BG of up to 1.9 eV. The introduction of sulfur into the support notably decreases the bandgap compared to CX-TiO_2, which has a band gap of 2.2 eV. Thus, the reduction in the BG value for the composites could be mainly attributed to the presence of the carbon support, due to electronic transitions between the carbon material and the different TiO2 phases, as well as its better light absorption capacity [39].

3.2 Adsorption and photocatalytic activity

The adsorption capacity of catalysts was analyzed until saturation in both dry and humid conditions under dark conditions, taking into account that the interactions between the carbon support and ethylene are based on physical adsorption. The adsorption breakthrough curves determined for the different materials are compared in Figures 3a and 3b and results are summarized in Table S2. TiO_2 presents a negligible adsorption capacity, related with the scarce porosity of this sample, as previously commented. On the contrary, carbon phases (CX and CXS) present a developed ethylene adsorption. As consequence, composites showed an intermediate performance in the ethylene removal by adsorption, associated mainly with the textural properties previously commented (Figure 3). Nevertheless, the influence of surface chemistry is also pointed out. Due to the non-polar nature of ethylene, the only type of attractive interactions between the carbon xerogels and the adsorbate are based on van der Waals forces, mainly π-π interactions between the double bond of ethylene and the aromatic character of the carbon supports [40-42]. Doping with sulfur negatively affected ethylene adsorption because it increased the polarity of the carbon adsorbents, while the ethylene molecule is nonpolar and presents low polarizability [42]. This is consistent with previous studies [43], which have reported that interactions between ethylene and carbon decreased in the presence of surface heteroatom groups, consequently reducing the adsorption capacity, as observed in CXS compared to CX (Figure 3a). The presence of humidity in the flow (Figure 3b) also decreases ethylene adsorption because adsorbed water partially blocks the porosity, reducing the number of adsorption sites available for ethylene.

After reaching saturation, the lamp was turned on to analyze the photocatalytic activity. The first series of photocatalytic tests were carried out under UV radiation to clearly evaluate the photo-activity of the samples (Figures 3c and d). Only CO_2 was detected as a reaction product, with the carbon balance (considering the stoichiometry of the reaction, equation (1) showing a deviation smaller than 5%.

$$C_2H_4 + 3O_2 \rightarrow 2CO_2 + 2H_2O \qquad (1)$$

Ethylene conversions are shown in terms of CO_2 formation. Despite doping and humidity hindering the interaction of ethylene with the catalysts surface, the photocatalytic performance of the composites is significantly enhanced by both parameters (Figures 3c-d). The improved performance of the composites after doping and under humid conditions (Figure 3d) could be related to the decrease in BG, as previously mentioned (Figure S4b). The new energy states of TiO_2 in the composites could enhance the formation of strongly oxidizing $HO^{\bullet}$ radicals, which subsequently oxidize ethylene [44]. The performance of the samples improves in the order of TiO_2 < CX-TiO_2 < CXS-TiO_2. In the absence of humidity, photooxidation performance decreased because the generation of hydroxyl radicals could be hindered, causing photocatalytic oxidation to proceed through less oxidizing radicals (such as superoxide radicals, $O_2^{\cdot -}$), which led to reduced activity [45].

Ethylene conversion also decreases when using Vis radiation compared to UV radiation (Figure 3e). In this case, experiments were conducted only under humid conditions. The different performance between UV and Vis radiation is more pronounced with the TiO_2 sample, which, as expected, shows very low activity under Vis radiation. The reduction of the band gap in composites, particularly in the sulfur-doped composite (i.e., CXS-TiO_2), enables these materials to function as active photocatalysts under Vis radiation.

Both composites exhibited better performance in comparison to TiO_2 (Figure 3e). This improvement can be explained by the synergistic effect between carbon and the TiO_2 matrix. The combination of carbon material and TiO_2 phases resulted in narrower band gap values, higher light absorption, and an increased lifespan of charge carriers by reducing electron-hole pair recombinations through charge separation within its π structure, thereby enhancing the overall photocatalytic activity [17, 46]. In the case of the sulfur-doped composite (CXS-TiO_2), an additional advantage is provided by the mobility of sulfur species from the support to the active phase, which generates new energy states in the semiconductor band structure associated with the formation of Ti-O-S bonds, as indicated by XPS analysis, and play a role in reducing the bandgap of this composite (Figure 2).

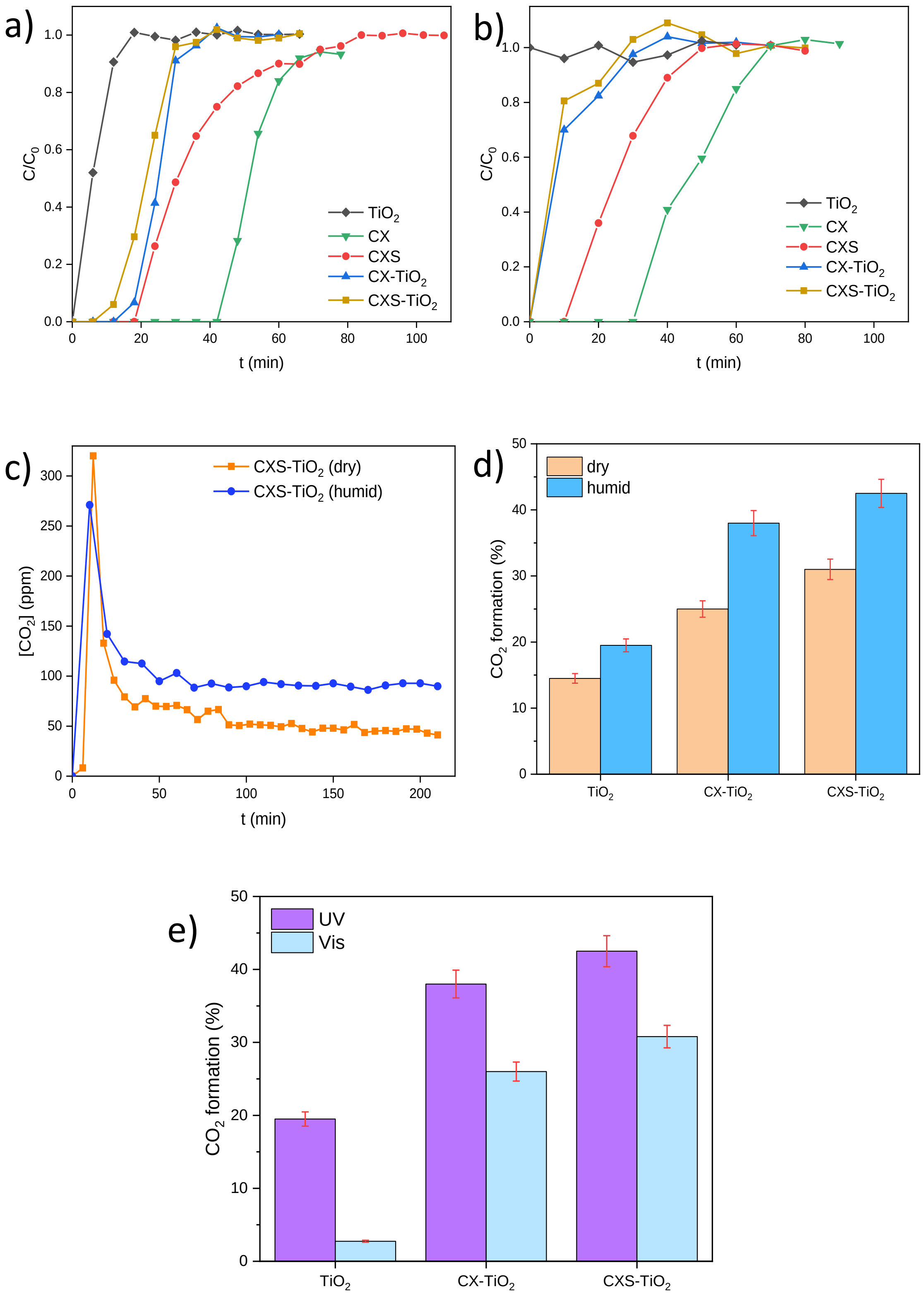

Figure 3. Ethylene adsorption of the materials under a) dry conditions, and b) humid conditions c) CO_2 formation in dry and humid conditions, under UV radiation for the CXS-TiO_2 composite; d) Comparison of CO_2 formation for all materials under dry and humid conditions under UV

radiation; e) CO_2 formation during ethylene degradation for the materials under humid conditions (comparison between UV and Vis radiation).

Several parameters can also contribute to the different performance of the samples. The interactions between the catalyst surface and the reactants, in this case, ethylene, are influenced by the combination of pore size distribution (PSD) and surface chemistry effects. Ethylene adsorption capacity is strongly favored after generating the composite, but decreases as the polar character of the surface increases or in the presence of moisture. Crystallographic factors are also important to consider. The transformation from anatase to rutile is accompanied by an increase of crystal size; large rutile crystals were detected on TiO_2. However, this transformation becomes progresively more difficult for the supported phases on CX-TiO_2 and especially CXS-TiO_2. Photocatalytic activity tends to improve with a decrease in particle size because, in this sense, also decreases the distance that photogenerated electrons and holes must travel to reach the surface of the crystal, making them more accessible to the reactants. As the pathway increases, the possibility of recombination increases as well. This principle underlies the development of photocatalysts based on TiO_2 nanoparticles.

4. Conclusions

In summary, sulfur-functionalities were introduced by using thiophene-2-carboxaldehyde as a polymerizing agent with resorcinol molecules during the preparation of carbon xerogels. The materials were impregnated *in-situ* with a TiO_2 precursor and then, carbonized to yield carbon/TiO_2 composites. During this process, a significant fraction of sulfur species migrates to the oxide phase, generating new energetic states that reduce the BG of the prepared semiconductors. Simultaneously, the stronger interactions between phases avoid sintering and the complete transformation into rutile. As a result, carbon/TiO_2 composites were obtained with well-dispersed TiO_2 nanoparticles featuring a mixture of anatase and rutile phases with smaller BG values. The synergistic effect between the carbon support and anatase/rutile phases doped with sulfur enables to obtain catalysts that are active under Vis radiation. The photooxidation of ethylene was improved by 25% and in the presence of humidity, compared to bare TiO_2. The

$CXS-TiO_2$ composite exhibited the best performance, which can be attributed to the dominant anatase phase in the material, induced by the incorporation of sulfur. Both carbon support and anatase/rutile phases doped with sulfur likely enhanced the formation of highly reactive $HO^{\bullet}$ radicals, although they also reduced ethylene adsorption. The reactions proceed selectively to CO_2 without producing any intermediate compounds, and no deactivation processes were observed.

Acknowledgements

This work was financially supported by projects with ref. PID2021-126579OB-C31 by MICIU/AEI/10.13039 /501100011033 and "ERDF A way of making Europe", ref. PCI2020-112045 funded by MICIU/AEI/ 10.13039/501100011033 and "European Union Next Generation EU/PRTR", as part of the PRIMA Programme (Nano4Fresh project), and by Junta de Andalucía - Consejería de Universidad, Investigación e Innovación - Project (P21_00208). L.T.P.-P. (FPU22/01255) and S.M.-T. (RYC-2019-026634-I) are grateful to MICIN/AEI/10.13039/501100011033 and FSE "El FSE invierte en tu futuro" for their FPU predoctoral and Ramon y Cajal research contracts, respectively. "Unidad de Excelencia Química Aplicada a Biomedicina y Medioambiente" of the University of Granada (UEQ-UGR) is gratefully acknowledged for the technical assistance.

References

[1] S.S. Hussain, O. Omelianovych, L.L. Larina, E. Park, V.T. Nguyen, B.T. Trinh, I. Yoon, H.-S. Choi, Black titania coated glass fiber as a photo absorber in interfacial solar steam generation under harsh condition, Solar Energy Materials and Solar Cells, 271 (2024), pp. 112829.

[2] M. Soleimani, J.B. Ghasemi, A. Badiei, Black titania; novel researches in synthesis and applications, Inorganic Chemistry Communications, 135 (2022), pp. 109092.

[3] H. Hamad, E. Bailón-García, F.J. Maldonado-Hódar, A.F. Pérez-Cadenas, F. Carrasco-Marín, S. Morales-Torres, Synthesis of TixOy nanocrystals in mild synthesis conditions for the degradation of pollutants under solar light, Applied Catalysis B: Environmental, 241 (2019), pp. 385-392.

[4] Y. Ao, J. Xu, D. Fu, C. Yuan, Preparation of Ag-doped mesoporous titania and its enhanced photocatalytic activity under UV light irradiation, Journal of Physics and Chemistry of Solids, 69 (2008), pp. 2660-2664.
[5] Z. Li, Y. Chu, T. Mi, J. Zhao, F. Meng, Enhanced photocatalytic H_2 evolution over conjugated polymer/Au@TiO_2 ternary heterojunction under visible light: Enriched photons input from polymers, Colloids and Surfaces A: Physicochemical and Engineering Aspects, 692 (2024), pp. 133991.
[6] M.R. Bayati, A.Z. Moshfegh, F. Golestani-Fard, On the photocatalytic activity of the sulfur doped titania nano-porous films derived via micro-arc oxidation, Applied Catalysis A: General, 389 (2010), pp. 60-67.
[7] Y. Zhao, N. Yang, T. Zhou, W. Zhan, J. Zhao, M. Chen, T. He, J. Zhang, Y. Zhang, G. Zhang, Q. Liu, Mechanism and performance of photocatalytic H_2 evolution for carbon self-doped TiO_2 derived from MIL-125, International Journal of Hydrogen Energy, 65 (2024), pp. 151-157.
[8] H. Hamad, E. Bailón-García, S. Morales-Torres, F. Carrasco-Marín, A.F. Pérez-Cadenas, F.J. Maldonado-Hódar, Functionalized cellulose for the controlled synthesis of novel carbon–Ti nanocomposites: Physicochemical and photocatalytic properties, Nanomaterials, 10 (2020), pp. 729.
[9] R. Chen, Y.-Y. Wang, X. Jiang, M.-H. Ji, K.-X. Li, H.-Y. Shi, H.-L. Wang, Y.-X. Chen, C.-Z. Lu, Lotus pollen-derived nitrogen and phosphorus self-doped TiO_2/carbon materials for photoelectrochemical application, Journal of Environmental Chemical Engineering, 12 (2024), pp. 112743.
[10] T. Umebayashi, T. Yamaki, H. Itoh, K. Asai, Band gap narrowing of titanium dioxide by sulfur doping, Applied Physics Letters, 81 (2002), pp. 454-456.
[11] T. Boningari, S.N.R. Inturi, M. Suidan, P.G. Smirniotis, Novel one-step synthesis of sulfur doped-TiO_2 by flame spray pyrolysis for visible light photocatalytic degradation of acetaldehyde, Chemical Engineering Journal, 339 (2018), pp. 249-258.
[12] S.A. Bakar, C. Ribeiro, A comparative run for visible-light-driven photocatalytic activity of anionic and cationic S-doped TiO_2 photocatalysts: A case study of possible sulfur doping through chemical protocol, Journal of Molecular Catalysis A: Chemical, 421 (2016), pp. 1-15.
[13] R.T. Bento, O.V. Correa, R.A. Antunes, M.F. Pillis, Surface properties enhancement by sulfur-doping TiO_2 films, Materials Research Bulletin, 143 (2021), pp. 111460.
[14] L.M. Pastrana-Martínez, S. Morales-Torres, V. Likodimos, J.L. Figueiredo, J.L. Faria, P. Falaras, A.M.T. Silva, Advanced nanostructured photocatalysts based on reduced graphene oxide–TiO_2 composites for degradation of diphenhydramine pharmaceutical and methyl orange dye, Applied Catalysis B: Environmental, 123-124 (2012), pp. 241-256.

[15] L.M. Pastrana-Martínez, S. Morales-Torres, V. Likodimos, P. Falaras, J.L. Figueiredo, J.L. Faria, A.M.T. Silva, Role of oxygen functionalities on the synthesis of photocatalytically active graphene–TiO2 composites, Applied Catalysis B: Environmental, 158-159 (2014), pp. 329-340.

[16] L.M. Pastrana-Martínez, S. Morales-Torres, S.K. Papageorgiou, F.K. Katsaros, G.E. Romanos, J.L. Figueiredo, J.L. Faria, P. Falaras, A.M.T. Silva, Photocatalytic behaviour of nanocarbon–TiO_2 composites and immobilization into hollow fibres, Applied Catalysis B: Environmental, 142-143 (2013), pp. 101-111.

[17] A.M. Regadera-Macías, S. Morales-Torres, L.M. Pastrana-Martínez, F.J. Maldonado-Hódar, Ethylene removal by adsorption and photocatalytic oxidation using biocarbon–TiO_2 nanocomposites, Catalysis Today, 413-415 (2023), pp. 113932.

[18] E. Bailón-García, A. Elmouwahidi, F. Carrasco-Marín, A.F. Pérez-Cadenas, F.J. Maldonado-Hódar, Development of Carbon-ZrO_2 composites with high performance as visible-light photocatalysts, Applied Catalysis B: Environmental, 217 (2017), pp. 540-550.

[19] C. Moreno-Castilla, F.J. Maldonado-Hódar, Synthesis and surface characteristics of silica– and alumina–carbon composite xerogels, Physical Chemistry Chemical Physics, 2 (2000), pp. 4818-4822.

[20] K.Y. Perera, S. Jaiswal, A.K. Jaiswal, A review on nanomaterials and nanohybrids based bio-nanocomposites for food packaging, Food chemistry, 376 (2022), pp. 131912.

[21] C. Mahendra, P.M. Sathya Sai, C. Anand Babu, K. Revathy, K.K. Rajan, Analysis and modeling of fixed bed sorption of cesium by AMP-PAN, Journal of Environmental Chemical Engineering, 3 (2015), pp. 1546-1554.

[22] W. Kiciński, M. Norek, A. Dziura, M. Polański, Copolycondensation of heterocyclic aldehydes: A general approach to sulfur and nitrogen dually-doped carbon gels, Microporous and Mesoporous Materials, 225 (2016), pp. 198-209.

[23] S. Cheng, X. Ding, X. Dong, M. Zhang, X. Tian, Y. Liu, Y. Huang, B. Jin, Immigration, transformation, and emission control of sulfur and nitrogen during gasification of MSW: Fundamental and engineering review, Carbon Resources Conversion, 6 (2023), pp. 184-204.

[24] M. Zukalová, M. Vinarčíková, B. Pitňa Lásková, L. Kavan, TiO_2 top layer improving the performance of sulfur/carbon composite cathode in Li-sulfur cells, Materials Chemistry and Physics, 296 (2023), pp. 127246.

[25] K. Soni, N. Lakshmi, R. Jain, A. Rani Chandra, A. Sheikh, Study of Sulphur doped TiO_2 dye sensetized solar cell, Materials Today: Proceedings, 29 (2020), pp. 275-277.

[26] L.O.A. Salim, M.Z. Muzakkar, A. Zaeni, M. Maulidiyah, M. Nurdin, S.N. Sadikin, J. Ridwan, A.A. Umar, Improved photoactivity of TiO_2 photoanode of dye-sensitized solar cells by sulfur doping, Journal of Physics and Chemistry of Solids, 175 (2023), pp. 111224.

[27] F. Rouquerol, J. Rouquerol, K.S.W. Sing, Adsorption by powders and porous solids principles, methodology and applications, Academic Press, London, 1999.

[28] T.A. Kandiel, L. Robben, A. Alkaima, D. Bahnemann, Brookite versus anatase TiO_2 photocatalysts: Phase transformations and photocatalytic activities, Photochemical & Photobiological Sciences, 12 (2013), pp. 602-609.

[29] K.-Y. Lee, K. Sato, A.R. Mohamed, Facile synthesis of anatase-rutile TiO_2 composites with enhanced CO_2 photoreduction activity and the effect of Pt loading on product selectivity, Materials Letters, 163 (2016), pp. 240-243.

[30] M. Kosmulski, The significance of the difference in the point of zero charge between rutile and anatase, Advances in Colloid and Interface Science, 99 (2002), pp. 255-264.

[31] F. Maleki, G. Di Liberto, G. Pacchioni, pH- and facet-dependent surface chemistry of TiO_2 in aqueous environment from first principles, ACS Applied Materials and Interfaces, 15 (2023), pp. 11216-11224.

[32] D.C.S. Gloria, C.H.V. Brito, T.A.P. Mendonça, T.R. Brazil, R.A. Domingues, N.C.S. Vieira, E.B. Santos, M. Gonçalves, Preparation of TiO_2/activated carbon nanomaterials with enhanced photocatalytic activity in paracetamol degradation, Materials Chemistry and Physics, 305 (2023), pp. 127947.

[33] K.M. Eblagon, A. Arenillas, A. Malaika, M. Fernando R. Pereira, J.L. Figueiredo, The influence of the surface chemistry of phosphorylated carbon xerogel catalysts on the production of HMF from fructose in water, Fuel, 334 (2023), pp. 126610.

[34] W. Zhang, N. Luo, S. Huang, N.-L. Wu, M. Wei, Sulfur-doped anatase TiO_2 as an anode for high-performance sodium-ion batteries, ACS Applied Energy Materials, 2 (2019), pp. 3791-3797.

[35] W. Kiciński, A. Dziura, Heteroatom-doped carbon gels from phenols and heterocyclic aldehydes: Sulfur-doped carbon xerogels, Carbon, 75 (2014), pp. 56-67.

[36] A.C. Breeson, G. Sankar, G.K.L. Goh, R.G. Palgrave, Phase quantification by X-ray photoemission valence band analysis applied to mixed phase TiO2 powders, Applied Surface Science, 423 (2017), pp. 205-209.

[37] J. Li, Q. Zhang, L. Zeng, D. He, Synthesis, characterization and photocatalytic study of graphene oxide and cerium co-doped in TiO_2, Applied Physics A, 122 (2016), pp. 51.

[38] G. Žerjav, K. Žižek, J. Zavašnik, A. Pintar, Brookite vs. rutile vs. anatase: What's behind their various photocatalytic activities?, Journal of Environmental Chemical Engineering, 10 (2022), pp. 107722.

[39] M. Pedrosa, L.M. Pastrana-Martínez, M.F.R. Pereira, J.L. Faria, J.L. Figueiredo, A.M.T. Silva, N/S-doped graphene derivatives and TiO2 for catalytic ozonation and photocatalysis of water pollutants, Chemical Engineering Journal, 348 (2018), pp. 888-897.

[40] W. Liang, Y. Zhang, X. Wang, Y. Wu, X. Zhou, J. Xiao, Y. Li, H. Wang, Z. Li, Asphalt-derived high surface area activated porous carbons for the effective adsorption separation of ethane and ethylene, Chemical Engineering Science, 162 (2017), pp. 192-202.

[41] F. Anwar, M. Khaleel, K. Wang, G.N. Karanikolos, Selectivity tuning of adsorbents for ethane/ethylene separation: A review, Industrial & Engineering Chemistry Research, 61 (2022), pp. 12269-12293.

[42] S. Schmittmann, C. Pasel, M. Luckas, D. Bathen, Adsorption of light alkanes and alkenes on activated carbon and zeolite 13X at low temperatures, Journal of Chemical & Engineering Data, 65 (2020), pp. 706-716.

[43] Y.-H. Wang, S. Bayatpour, X. Qian, B. Frigo-Vaz, P. Wang, Activated carbon fibers via reductive carbonization of cellulosic biomass for adsorption of nonpolar volatile organic compounds, Colloids and Surfaces A: Physicochemical and Engineering Aspects, 612 (2021), pp. 125908.

[44] N. Pugazhenthiran, H. Valdés, R.V. Mangalaraja, P. Sathishkumar, S. Murugesan, Graphene modified "black {001} TiO_2" nanosheets for photocatalytic oxidation of ethylene: The implications of chemical surface characteristics in the reaction mechanism, Separation and Purification Technology, 292 (2022), pp. 121008.

[45] Z. Rao, G. Lu, L. Chen, A. Mahmood, G. Shi, Z. Tang, X. Xie, J. Sun, Photocatalytic oxidation mechanism of gas-phase VOCs: Unveiling the role of holes, $^{\bullet}OH$ and $^{\bullet}O_2^-$, Chemical Engineering Journal, 430 (2022), pp. 132766.

[46] M. Huang, J. Lin, R. Li, Y. Su, X. Zhao, Y. Liu, W.J. Chen, X. Lian, X. Chen, X. Pan, Hierarchical ZnO nanosheet-reduced graphene oxide composites for photocatalytic ethylene oxidation, ACS Applied Nano Materials, 5 (2022), pp. 1828-1835.